Article

Small Bioactivated Magnetic Quantum Dot Micelles

Victor Roullier, Fabien Grasset, Fouzia Boulmedais,
Franck Artzner, Olivier Cador, and Vale#rie Marchi-Artzner

More About This Article

Additional resources and features associated with this article are available within the HTML version:

- Supporting Information
- Access to high resolution figures
- Links to articles and content related to this article
- Copyright permission to reproduce figures and/or text from this article

View the Full Text HTML

Small Bioactivated Magnetic Quantum Dot Micelles

Victor Roullier,[†] Fabien Grasset,[†] Fouzia Boulmedais,[†,‡] Franck Artzner,[§] Olivier Cador,[†] and Valérie Marchi-Artzner*,[†]

Sciences Chimiques de Rennes, University Rennes 1, CNRS UMR 6226, Rennes, France, Institut Charles Sadron, CNRS UPR 22, Strasbourg, France, and Institut de Physique de Rennes, University Rennes 1, CNRS UMR 6251, Rennes, France

Many biological processes are activated through nondiffusive distribution of biomolecules in biological systems. To both label and induce such gradients of proteins, our strategy is to prepare bioactivated nanometer-sized nanoparticles combining magnetic and fluorescent properties. Here, bioactivated fluorescent magnetic micelles with an hydrodynamic diameter of around 25 nm are obtained by coencapsulation of both hydrophobic CdSe/ZnS quantum dots (QD) and γ-Fe$_2$O$_3$ nanocrystals into a liquid crystal phase composed of synthetic amphiphilic PEG gallates derivatives bearing a terminal active chemical group. The present method permits to both functionalize and solubilize magnetic and fluorescent nanocrystals into the same micelle starting from a condensed hybrid hexagonal phase. Reactive groups, such as amine, carboxylic acid, and biotin, are introduced on the surface of the nanoparticle with a controlled molar ratio. The magnetic and fluorescence properties are demonstrated by complementary techniques such as SQUID experiments and fluorescence spectrometry. The molar QD/γ-Fe$_2$O$_3$ ratio between quantum dots and iron oxide nanocrystals is optimized to the value 1/1 to get a fluorescence quantum yield of 15% and to keep magnetic properties. The fluorescent magnetic micelles can move and be trapped under a magnetic field gradient in a few minutes. Finally, the synthesis of various gallate ligands bearing a biotin terminal group permits to bioactivate the nanocrystals as demonstrated by the selective binding of the micelles to agarose Streptavidin micrometer-range beads. These multifunctional fluorescent and magnetic nanoparticles of small size can target any biomolecule through biotin/streptavidin or amide covalent binding and could be used to manipulate and vary its spatial distribution under a magnetic gradient field.

Introduction

Many biological self-organized phenomena in cells such as the formation of the cytoskeleton or signal transduction pathways result from the regulation of the dynamical self-assemblies of molecules through the fine-tuning of signaling pathways in time and space.[1] To modulate these phenomena, the idea is to generate protein concentration gradients to localize spatially specific target proteins. In this view, fluorescent magnetic nanoparticles could permit us to both follow and trap a protein to activate any biological process sensitive to concentration gradients such as Actin or microtubule polymerization. Very few reported research works concern a synergic effect of both fluorescent and magnetic properties to address a biological question. In most of the cases, the nanoparticle function appears to be limited to the rule of passive reporter of tagged biomolecule or drug. Recently, magnetic nanoparticles were shown to activate a biochemical signaling mechanism resulting in calcium influx

in cells. This signal transduction is normally switched on by ligand multibinding of the membrane via receptor clustering.[2]

Here is described the preparation of new bioactivated fluorescent and magnetic nanoparticles of well-defined size as a first step toward the generation of proteins gradients under magnetic field. In one hand, fluorescent quantum dots (QD) are selected for their robust optical properties and their well-defined size.[3] Their fluorescence properties include high quantum yield, photostability, and emission wavelength tunable with their size.[4] QD are specially functionalized for tracking, labeling of an individual biomolecule and in vitro or in vivo imaging.[5–8] Iron oxide nanoparticles are also used

* Corresponding author. Address: Sciences Chimiques de Rennes, CNRS UMR 6226, Campus Beaulieu-Université de Rennes 1, 263 Av du Général Leclerc, 35042 Rennes cedex, France. Tel.: 33 (0)2 23 23 56 48. Fax: 33 (0)2 23 23 67 38. E-mail: valerie.marchi-artzner@univ-rennes1.fr.
  † Sciences Chimiques de Rennes, University Rennes 1.
  ‡ Institut Charles Sadron.
  § Institut de Physique de Rennes, University Rennes 1.

(1) Bastiaens, P.; Caudron, M.; Niethammer, P.; Karsenti, E. *Trends Cell Biol.* **2006,** *16* (3), 125–134.

(2) Mannix, R. J.; Kumar, S.; Cassiola, F.; Montoya-Zavala, M.; Feinstein, E.; Prentiss, M.; Ingber, D. E. *Nat. Nanotechnol.* **2008,** *3* (1), 36–40.

(3) Murray, C. B.; Kagan, C. R.; Bawendi, M. G. *Annu. Rev. Mater. Sci.* **2000,** *30,* 545–610.

(4) Somers, R. C.; Bawendi, M. G.; Nocera, D. G. *Chem. Soc. Rev.* **2007,** *36* (4), 576–591.

(5) Goldmann, E. R.; Uyada, H. T.; Hayhurst, A.; Mattoussi, H. Quantum Dots: Applications in Biology; Hotz, C. Z., Bruchez, M., Eds.; Methods in Molecular Biology; Springer: New York, 2007; Vol. 374, pp 207–227.

(6) Dif, A.; Henry, E.; Artzner, F.; Baudy-Floc'h, M.; Schmutz, M.; Dahan, M.; Marchi-artzner, V. *J. Am. Chem. Soc.* **2008,** *130* (26), 8289–8296.

(7) Ben, N. G.; Giepmans, S. R. A.; Ellisman, M. H.; Tsien, R. Y. *Science* **2006,** *312,* 217–224.

(8) Yu, W. W.; Chang, E.; Falkner, J. C.; Zhang, J.; Al-Somali, A. M.; Sayes, C. M.; Johns, J.; Drezek, R.; Colvin, V. L. *J. Am. Chem. Soc.* **2007,** *129* (10), 2871–2879.

in the biomedical field, as a contrast agent in magnetic resonance imaging[9] (MRI) in vivo, in the hyperthermia treatment of cancers[10,11] and also for magnetic separation[12] and guiding.[13] Various approaches have extensively been attempted to combine both fluorescent semiconductor (CdSe, ZnS, CdTe, ZnO, CdO, NiO) and magnetic (Co, Mn, Ni, Fe) properties within an unique nanocrystal. Alternative strategies have been developed to combine QD and magnetic particles together using densely packed emulsion droplet,[14,15] silica encapsulation,[16−21] polymer or polyelectrolyte encapsulation,[12,22−26] giant vesicles[27] and micellization.[28] Nevertheless the size of the fluorescent magnetic nanoparticles described in the literature is rather large, i.e., several hundred nanometers.[20] To use these nanoparticles as active probe, it is crucial to control their size because the cellular response is size-dependent.[29]

To prepare hybrid magnetic and fluorescent nanoparticles, we selected synthetic pegylated gallate amphiphiles to encapsulate hydrophobic QDs and iron oxide nanocrystals.[30] It was previously demonstrated that these amphiphiles self-organize into micelles with a hydrodynamic diameter of around 25 nm. These micelles are obtained by a simple water dilution starting from an hybrid hexagonal phase composed of nanocrystals and PEG gallate amphiphiles. Here we optimized the chemical structure to improve the colloidal stability and to introduce a terminal functional group such as amine, carboxylic acid, or biotin to bind to a biomolecule. Hybrid micelles with a controlled number of terminal chemical functions are obtained starting from a mixture containing different functionalized amphiphiles. The magnetic, optical, and colloidal properties of these hybrid micelles are characterized by complementary techniques including optical and electron microscopy, dynamic light scattering, gel electrophoresis, and magnetometer experiments. As an illustration of their chemical recognition properties, specific adhesion of biotin hybrid micelles is shown on Streptavidin-coated agarose microbeads. The collective trapping of these hybrid nanoparticles is directly followed by optical fluorescence microscopy. Thus the synergic effect of magnetic and fluorescent properties is demonstrated by moving them under magnetic field induced by a permanent magnet.

Experimental Section

General Prodecures. All the organic gallate amphiphile ligands are synthesized at the laboratory (see the Supporting Information). Core−shell CdSe/ZnS quantum dots (QD) are produced according to the previously described two-step organometallic synthesis at high temperature.[31−35] 1-Tetradecylphosphonic acid and hexadecylamine were purchased from Alfa-Aesar, all the other compounds were purchased from Sigma-Aldrich.

Synthesis of the Nanocrystals. The synthesis of the nanocrystals permits to reach a broad emission wavelength range (from 520 to 617 nm, see typical protocol in the Supporting Information). The optical properties of the QD, i.e. concentration and fluorescence quantum yield, are estimated from the molar extinction coefficients calculated according to the literature.[36,37]

Superparamagnetic γ-Fe_2O_3 nanocrystals are synthesized according to a high temperature nucleation and growth process.[38] Shape and size of nanoparticles are characterized by TEM and their magnetic properties by SQUID device. A ligand exchange step is performed in chloroform (1 mL) overnight with 3 mmol of trioctylphosphine oxide and 6.7 nmol of γ-Fe_2O_3 particles. Then methanol (4 mL) is added and the mixture is centrifuged (20000 g, 10 min). After removal of supernatant, the nanoparticles are solubilized in chloroform (1 mL). The iron concentration of the magnetic nanocrystals is estimated by inductively coupled plasma optical emission spectroscopy (ICP-OES) after a nitric acid dissolution and a water dilution.

Micellization of the Nanocrystals. Amphiphilic ligands, QD, and γ-Fe_2O_3 nanocrystals are incorporated into a nonpolar organic solvent before drying under a 100 mbar vacuum. The micellization

(9) Mornet, S.; Vasseur, S.; Grasset, F.; Duguet, E. *J. Mater. Chem.* **2004**, *14*, 2167–2175.

(10) Jordan, A.; Scholz, R.; Wust, P.; Fahling, H.; Roland, F. *J. Magn. Magn. Mater.* **1999**, *201* (1−3), 413–419.

(11) Baker, I.; Zeng, Q.; Li, W.; Sullivan, C. R. *J. Appl. Phys.* **2006**, *99*, 08H106.

(12) Wang, G.-P.; Song, E.-Q.; Xie, H.-Y.; Zhang, Z.-L.; Tian, Z.-Q.; Zuo, C.; Pang, D.-W.; Wu, D.-C.; Shi, Y.-B. *Chem. Commun.* **2005**, (34), 4276–4278.

(13) Lu, A. H.; Salabas, E. L.; Schüth, F. *Angew. Chem., Int. Ed.* **2007**, *46* (8), 1222–1244.

(14) Mandal, S. K.; Lequeux, N.; Rotenberg, B.; Tramier, M.; Fattaccioli, J.; Bibette, J.; Dubertret, B. *Langmuir* **2005**, *21* (9), 4175–4179.

(15) Mandal, S. K. *J. Magn. Magn. Mater.* **2007**, *311* (1), 88–91.

(16) Yi, D. K.; Selvan, S. T.; Lee, S. S.; Papaefthymiou, G. C.; Kundaliya, D.; Ying, J. Y. *J. Am. Chem. Soc.* **2005**, *127* (14), 4990–4991.

(17) Salgueiriño-Maceira, V.; Correa-Duarte, M. A.; Spasova, M.; Liz-Marzán, L. M.; Farle, M. *Adv. Funct. Mater.* **2006**, *16* (4), 509–514.

(18) Kim, J.; Lee, J. E.; Lee, J.; Yu, J. H.; Kim, B. C.; An, K.; Hwang, Y.; Shin, C. H.; Park, J. G.; Kim, J.; Hyeon, T. *J. Am. Chem. Soc.* **2006**, *128* (3), 688–689.

(19) Sathe, T. R.; Agrawal, A.; Nie, S. *Anal. Chem.* **2006**, *78* (16), 5627–5632.

(20) Insin, N.; Tracy, J. B.; Lee, H.; Zimmer, J. P.; Westervelt, R. M.; Bawendi, M. G. *ACS Nano* **2008**, *2* (2), 197–202.

(21) Salgueiriño-Maceira, V.; Correa-Duarte, M. A. *Adv. Mater.* **2007**, *19* (23), 4131–4144.

(22) Lee, J.; Lee, Y.; Youn, J. K.; Na, H. B.; Yu, T.; Kim, H.; Lee, S. M.; Koo, Y. M.; Kwak, J. H.; Park, H. G.; Chang, H. N.; Hwang, M.; Park, J. G.; Kim, J.; Hyeon, T. *Small* **2008**, *4* (1), 143–152.

(23) Gaponik, N.; Radtchenko, I. L.; Sukhorukov, G. B.; Rogach, A. L. *Langmuir* **2004**, *20* (4), 1449–1452.

(24) Xie, H. Y.; Zuo, C.; Liu, Y.; Zhang, Z. L.; Pang, D. W.; Li, X. L.; Gong, J. P.; Dickinson, C.; Zhou, W. *Small* **2005**, *1* (5), 506–509.

(25) Zebli, B.; Susha, A. S.; Sukhorukov, G. B.; Rogach, A. L.; Parak, W. J. *Langmuir* **2005**, *21* (10), 4262–4265.

(26) Hong, X.; Li, J.; Wang, M.; Xu, J.; Guo, W.; Li, J.; Bai, Y.; Li, T. *Chem. Mater.* **2004**, *16* (21), 4022–4027.

(27) Beaune, G.; Dubertret, B.; Clément, O.; Vayssettes, C.; Cabuil, V.; Ménager, C. *Angew. Chem., Int. Ed.* **2007**, *46* (28), 5421–5424.

(28) Mulder, W. J. M.; Koole, R.; Brandwijk, R. J.; Storm, G.; Chin, P. T. K.; Strijkers, G. J.; deMelloDonega, C.; Nicolay, K.; Griffioen, A. W. *Nano Lett.* **2006**, *6* (1), 1–6.

(29) Lin, C. A. J.; Sperling, R. A.; Li, J. K.; Yang, T. Y.; Li, P. Y.; Zanella, M.; Chang, W. H.; Parak, W. J. *Small* **2008**, *4* (3), 334–341.

(30) Boulmedais, F.; Bauchat, P.; Brienne, M. J.; Arnal, I.; Artzner, F.; Gacoin, T.; Dahan, M.; Marchi-Artzner, V. *Langmuir* **2006**, *22* (23), 9797–9803.

(31) Murray, C. B.; Norris, D. J.; Bawendi, M. G. *J. Am. Chem. Soc.* **1993**, *115* (19), 8706–8715.

(32) Dabbousi, B. O.; Rodriguez-Viejo, J.; Mikulec, F. V.; Heine, J. R.; Mattoussi, H.; Ober, R.; Jensen, K. F.; Bawendi, M. G. *J. Phys. Chem. B* **1997**, *101* (46), 9463–9475.

(33) Qu, L.; Peng, X. *J. Am. Chem. Soc.* **2002**, *124* (9), 2049–2055.

(34) Peng, X.; Schlamp, M. C.; Kadavanich, A. V.; Alivisatos, A. P. *J. Am. Chem. Soc.* **1997**, *119* (30), 7019–7029.

(35) Qu, L.; Yu, W. W.; Peng, X. *Nano Lett.* **2004**, *4* (3), 465–469.

(36) Leatherdale, C. A.; Woo, W. K.; Mikulec, F. V.; Bawendi, M. G. *J. Phys. Chem. B* **2002**, *106* (31), 7619–7622.

(37) Yu, W. W.; Qu, L.; Guo, W.; Peng, X. *Chem. Mater.* **2003**, *15* (14), 2854–2860.

(38) Sun, S.; Zeng, H.; Robinson, D. B.; Raoux, S.; Rice, P. M.; Wang, S. X.; Li, G. *J. Am. Chem. Soc.* **2004**, *126* (1), 273–279.

of the nanoparticles into water is obtained by hydration of the mixture in aqueous solution (buffer, saline solution or pure water) at 50 °C (5 min). The crude suspension is first centrifuged (20000 g, 10 min) to remove aggregates. Size exclusion chromatography (SEC) is then performed on NAP-10 disposable desalting columns (Sephadex, GE Healthcare) to eliminate ligand excess. After concentration on an ultrafiltration device Vivaspin 500 (10 000 MWCO, Polyethersulfone, Sartorius), this purified suspension of nanoparticles is then ultracentrifuged (at 120 000 g for 90 min, TL-100 Beckman Coulter) on a Saccharose gradient cushion (from 5 to 30% saccharose) to further purify and eliminate the empty gallate micelles. This ultracentrifugation is performed in a pH 8.5 saline borate buffer (20 mM boric acid and 150 mM NaCl).

Analysis and purification by HPLC are carried out on an ÄKTA-purifier-10 HPLC system monitored by Unicorn Manager 5.1 software with a detection of the 350 nm absorption of QD and γ-Fe$_2$O$_3$. A Superdex 200 GL column (10 × 300, 13 μm, Amersham Biosciences, France) is used with phosphate buffer saline as mobile phase (0.01 M phosphate buffer, 0.0027 M KCl, 0.137 M NaCl, pH 7.4) at flow rate of 0.5 mL/min. Absorbance is detected in situ during the separation.

Characterization of Hybrid Micelles. Absorbance measurements of QD solution are recorded by Cary 100 UV–visible scan spectrophotometer (Varian, Australia). Fluorescence properties of hybrid micelles are investigated with a Fluorolog-3 fluorescence spectrometer (FL3-22, Horiba Jobin Yvon). The QD solutions are excited at 350 nm. The fluorescence quantum yield of QD is calculated using the Rhodamine 6G (Molecular Probes Invitrogen) in ethanol as a reference.

Dynamic light scattering (DLS) is measured by collecting the scattered intensity at a 173° angle on a Zetasizer Nano-ZS (Malvern Instruments, England) apparatus at 25 °C. All the samples are filtrated through 0.2 μm Millipore filter (Millex GV, Sigma-Aldrich, France).
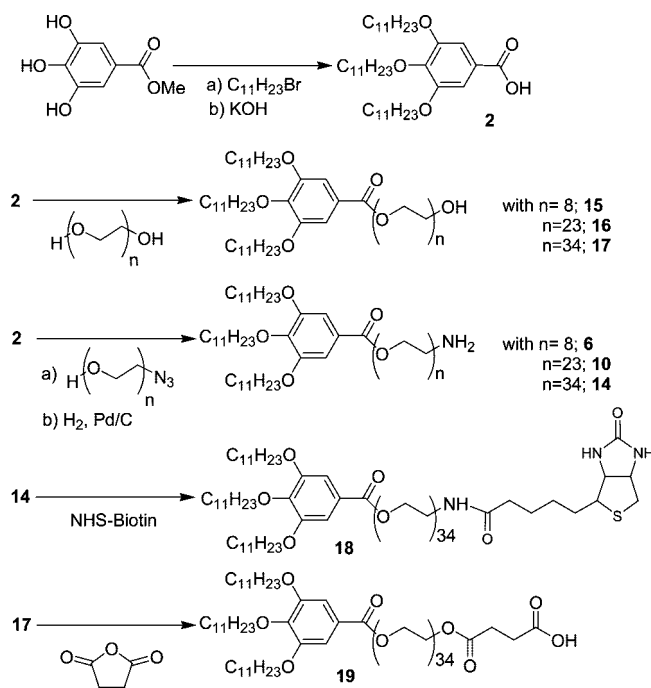
Transmission electron microscopy (TEM) samples are performed at the service of transmission electron microscopy of the University of Rennes 1. The samples are deposited on amorphous carbon film supported on a 300 mesh copper grid (Oxford Instruments, G2300C, England). The grids are observed in a Geol apparatus (voltage 120 kV).

The fluorescence optical microscopy observations are performed either under direct bright light and epifluorescence on an inverted microscope IX71 (Olympus, Japan) equipped with both a 4×, 0.1 (NA) and a 10×, 0.3 (NA) objectives (Olympus, Japan). QD are excited at 365 nm by a high vacuum mercury lamp (200 W). Images are acquired by a colorview II camera equipped with a soft imaging system (Olympus, Japan). The hybrid micelles are observed after addition into a closed aqueous compartment with or without a permanent cylindrical magnet (1.25 T, from Edmunds Optics) located onto the glass slide at a distance of some millimeters from the fluorescent front of the micelles.

Magnetic characterization is performed using a superconducting quantum interference device (SQUID). Zero-field-cooled (ZFC) and field-cooled (FC) magnetization curves are obtained between 5 and 300 K under an applied field of 100 G in the case of a suspension of γ-Fe$_2$O$_3$ nanoparticles and hybrid magnetic and fluorescent micelles.

Gel electrophoresis migrations are performed on a GEL XL ULTRA V-2 device (Labnet international Incorporation) using a 1% agarose gel with 0.03 M phosphate buffer (pH 5) performed under a 50 V electric field for 1 h. The pH is controlled by a C-931 electrochemical analyzer pHmeter (Consort), equipped with a Fisher Bioblock microprobe.

Scheme 1. Synthesis Route of the G$_{11}$EO$_n$Z (n = 8, 23, 34) Amphiphilic Compounds (with Z = Amino 14, Alcohol 17, Biotin Group 18 or Carboxylic Acid 19) Used for the Functionalization of the QDs

Binding of Hybrid Biotin γ-Fe$_2$O$_3$/QD Micelles to Streptavidin-Coated Microbeads. Immobilized Streptavidin agarose gel beads are purchased from Pierce. After dilution (4×) into a 150 mM saline solution, the beads suspension (50 μL) is centrifuged (4000 g, 30 s). After elimination of the supernatant, agarose beads are washed with saline solution (200 μL) and centrifuged twice. Hybrid micelles (80 μL, 100 nM) and immobilized Streptavidin beads (20 μL) are mixed together in a pH 8.5 borate buffer (12 μL, 200 nM) during 1 h under stirring. After washing and four centrifugations (4000 g, 30 s), the samples are observed with bright field (acquisition time 5 ms) and epifluorescence (acquisition time 300 ms) microscope with a 10× objective (Olympus).

Results and Discussion

Synthesis and Self-Organization of the Ligands in Water. In order to solubilize the nanoparticles into water, gallate amphiphiles composed of three undecanoyl aliphatic chains and a polyethyleneglycol (PEG) hydrophilic spacer grafted on the aromatic ring are selected (see Scheme 1). Our choice to use these amphiphilic gallates is motivated by their ability to form various liquid crystal phases and to encapsulate quantum dots. We have previously demonstrated that the G$_{12}$EO$_{34}$OH gallate amphiphile permits to prepare quantum dot micelles by simple dilution of an hybrid hexagonal phase into water.[30] The three long alkyl chains permits to optimize the van der Waals hydrophobic interactions with the trioctylphosphonic oxide (TOPO) hydrophobic ligands coating nanoparticles. Here the reduction in length of the alkyl chains to eleven carbons lowers the melting point of the amphiphiles in presence of water from 8−12 to 1.5 °C, as shown from differential scanning calorimetry analysis (DSC) (see Table A in the Supporting Information). Therefore, the crystallization of the chains in the lamellar phase is avoided due to the packing defects of the nonpeer number

Table 1. Structural Parameters of the Phases Adopted in the Presence of a Water Gradient Obtained from SAXS Technique

ligand	nature and structural parameters of the adopted phases by increasing the water ratio			
15 ($n = 8$)	hexagonal (indirect) 54−61 Å	cubic *Ia3d* 133−149 Å	hexagonal (direct) 70 Å	micelles
16 ($n = 23$)	lamellar 61−89 Å	cubic *Ia3d* 216−225 Å	rectangular 109/180−112/183 Å	hexagonal (direct) 119−128 Å	micelles
17 ($n = 34$)	lamellar 89 Å	cubic *Ia3d* 219−223 Å	rectangular 100/183−109/185 Å	hexagonal (direct) 112−126 Å	micelles

of carbon atoms in the chains. In addition, PEG polymers are well-known to hindrance the nonspecific interactions with cellular membranes, decreasing the nonspecific adsorption and increasing the circulation lifetime of the colloids in biological organism.[39] Here the number of PEG units is adjusted in order to equilibrate the ratio between the volume of the hydrophobic chains and the area of the hydrophilic PEG polar headgroup which defines the formation and the curvature of the micelles. To produce the smallest micelles capable to encapsulate fluorescent and magnetic particles, three different lengths of the PEG spacer units ($n = 8, 23, 34$) are selected. Finally, functional terminal groups such as an amine, a carboxylic acid, or biotin are grafted to conjugate the obtained nanoparticle micelles to a biomolecule by either classical coupling via activated ester or specific recognition with Streptavidin. To synthesize the compounds presented in Scheme 1, three undecanoyl chains are grafted on the commercially available methyl gallate ester and then a polyethyleneglycol (PEG) polymer of various lengths is condensed by esterification on the acid **2** to give the alcohol gallate ester amphiphiles **15**, **16**, and **17**. The terminal alcohol function is converted into an amine via the azide compound to provide the final amine compounds **6**, **10**, and **14**. The NHS-biotin activated ester is grafted on **14** by amidation to get the biotinylated ligand **18**. The carboxylic acid **19** is prepared by condensation of succinic anhydride on the alcohol gallate amphiphile **17**.

The phases adopted by the amphiphiles **15**, **16**, and **17** are identified by small-angle X-ray scattering (SAXS) and are reported in Table 1. In the presence of an increasing water ratio, the shortest pegylated ligand **15** shows successively an inverse hexagonal phase, a cubic *Ia3d* phase and then a short direct hexagonal phase and finally a micellar phase (Table 1). In the regime of low water dilution, hydrophilic head-groups are packed inside the columns and aliphatic chains are oriented outside of the column. As previously observed,[30] **17** forms successively a lamellar, a direct hexagonal phases through a cubic *Ia3d* phase in presence of an increased amount of water and gives finally a micellar phase under a regime of large water dilution (see SAXS diagrams in Figure A of the Supporting Information). The critical micellar concentrations (cmc) of **14** and **17** are found to be around 300 ± 50 nM by surface tension measurements (see Figure **B** in Supporting Information). The ligand **16** ($n = 23$) exhibits a complex behavior presenting a rectangular phase between cubic and direct hexagonal one. This distorted direct hexagonal phase facilitates the transition from a cubic to a hexagonal structure.

Nanoparticle Synthesis and Micellization Process. For the compounds described here, the solubilization of the hydrophobic quantum dots (TOPO-QD) into water is tested

by DLS measurements and optical microscopy. Most of the following experiments are performed with homemade nanocrystals. The magnetic γ-Fe$_2$O$_3$ nanocrystals are prepared according to Sun et al.[38] Their size is found to be about 4 ± 1.5 nm by TEM (see Figure 1a and the Supporting Information, Figure Ca). Their molar extinction coefficient ε in chloroform is found to be $1\,821\,000 \pm 1000$ mol L^{-1} cm^{-1} calculated from the absolute concentration of iron determined by ICP. The magnetic nanocrystals exhibit a classical superparamagnetic behavior as observed by superconducting quantum interference device (SQUID) (see Figure D in the Supporting Information).[13] A two-step synthesis of CdSe/ZnS quantum dots provides monodispersed fluorescent nanocrystals emitting from 525 to 605 nm.[32] A regular decay of the quantum yield is observed while nanocrystal diameter increases (80% for 525 nm, 49% for 541 nm, and 16% for 605 nm) and some experiments are conduced with Evident 605 nm QD. The size of the 605nm QD (QD$_{605}$) dispersed in chloroform is found to be around 5.0 ± 1.0 nm from transmission electronic microscopy (TEM) (see Figure 1b and the Supporting Information, Figure Cb).

Whereas the solubilization is impossible in the case of PEG with $n = 8$ (**15**), a phase transfer of the hydrophobic QDs occurs in the case of PEG with, respectively, $n = 23$ (**16**) and 34 (**17**). Nevertheless, in the case of **16** ($n = 23$), the polydispersity of the obtained micelles by encapsulation of the nanocrystals becomes very high as shown from DLS measurements (not shown). The structural analysis of the lyotropic phases of the various amphiphilic ligands **15**, **16** and **17** exhibits a correlation between their ability to solubilize hydrophobic quantum dots and the easier tendency to form micelles in excess of water starting from a direct hexagonal phase. Thus the amphiphilic ligand **17** offers the best conditions to obtain stable and monodisperse micelles without any heating step thanks to the reduction in length of the alkyl chains. In addition, the preparation of functional amine **14**, biotin **18**, and carboxylic acid **19** ligands permits us to consider further bioactivation.

To prepare functional nanocrystal micelles, we performed the encapsulation of both types of nanocrystals by water dilution of the hybrid direct hexagonal phase of **14/17** mixtures (ratio from 0:1 to 1:1). The size of the micelles is determined by dynamic light scattering (DLS) and transmission electron microscopy (TEM). After centrifugation and purification on gel filtration, two peaks are systematically detected by dynamic light scattering (DLS) the first one at 25 nm and the second one around 100 nm (see Figure E in the Supporting Information). The ratio of this latter peak represents less than 50% in the scattering intensity signal. This peak corresponds to a very small amount in number of aggregates in comparison of the micelles at 25 nm as the
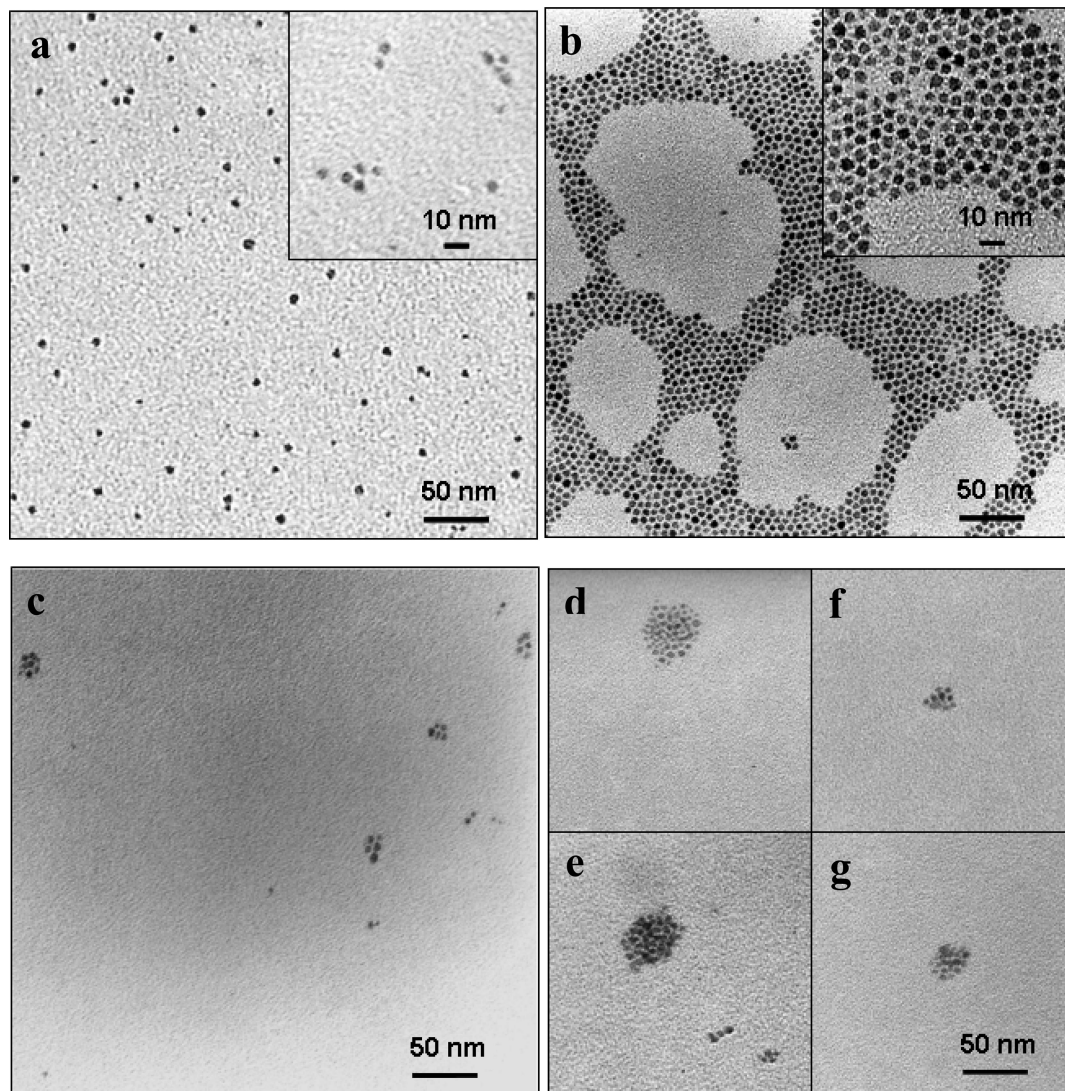
Figure 1. Transmission electron microscopy images of (a) QD_{605} in chloroform (mean inorganic diameter $D = 5.0 \pm 1.0$), (b) γ-Fe_2O_3 nanoparticles in chloroform ($D = 4 \pm 1.5$ nm), (c–g) γ-Fe_2O_3 /QD_{605} hybrid micelles in water prepared from a mixture of **14/17** (10:90).
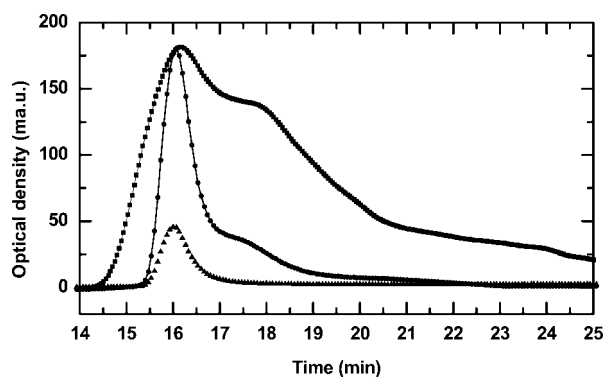

Figure 2. Size exclusion chromatogram of 10% amine (**14/17** 10:90) QD_{605} micelles before (at 220 nm, square) and after ultracentrifugation at 220 nm (QD_{605} and empty micelle absorption) (dot) and at 350 nm (QD_{605} absorption) (triangle).

light scattering intensity varies as r^6. To remove the empty micelles, a further purification by ultracentrifugation is performed. As shown by analytical size exclusion chromatography in Figure 2, the free ligands in excess and empty micelles detected from their absorption at 220 nm are almost removed after ultracentrifugation. In the same time, the

presence of the quantum dots is detected from their absorption at 350 nm. After ultracentrifugation, the final hydrodynamic diameter of the γ-Fe_2O_3/QD_{605} micelles determined by DLS, is found to be 25 ± 3.5 nm with a residual aggregates peak (corresponding to 30% in the scattered intensity signal), which is attributed to a dynamical exchange of the amphiphiles between hybrid γ-Fe_2O_3/QD_{605} micelles and the solution in equilibrium. Regarding the morphology of the micelles, only a small number of nanocrystals are encapsulated into one micelle as suggested from the TEM images obtained for γ-Fe_2O_3/QD_{605} hybrid micelles (Figure 1c–g), γ-Fe_2O_3 micelles (see Figure Fa in the Supporting Information) and QD_{605} micelles (see Figure Fb in the Supporting Information). Even if one can not exclude that the drying of the sample before TEM observation modifies the size distribution of the hybrid (**14/17** 10:90) micelles containing nanocrystals, each hybrid micelle appears to contain less than a few tens of nanocrystals.

(39) Kirchner, C.; Liedl, T.; Kudera, S.; Pellegrino, T.; MunozJavier, A.; Gaub, H. E.; Stolzle, S.; Fertig, N.; Parak, W. J. *Nano Lett.* **2005**, *5* (2), 331–338.
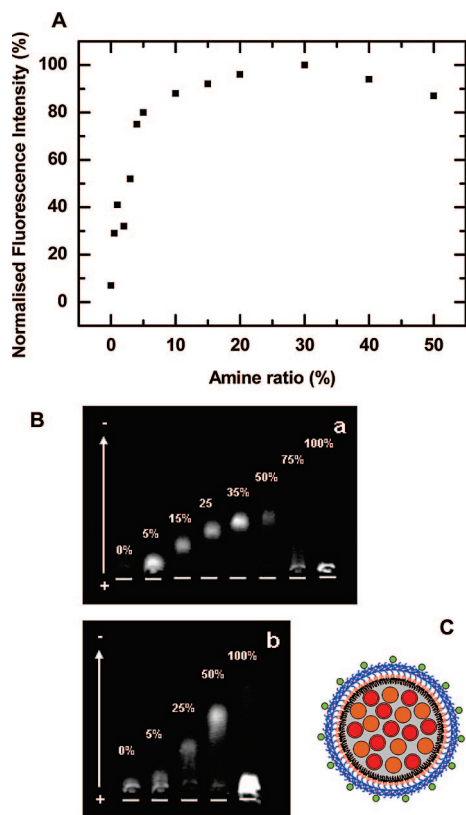
Figure 3. (A) Normalized fluorescence intensity of various charged QD$_{605}$ micelles prepared from a **14/17** mixture (from 0% of to 50% of **14** amine ligand). (B) Electrophoresis gels of various charged micelles with an increasing ratio of **14** containing either QD$_{605}$ alone (a) or γ-Fe$_2$O$_3$/QD$_{605}$ (b). (C) Schematic representation of an hybrid micelle (with QD$_{605}$ (red), γ-Fe$_2$O$_3$ (brown) prepared from a mixture of **14** (green dots) and **17**.

To control the surface concentration of functional groups on the QD surface, the amine/alcohol ratio is systematically varied from 0 to 50% of **14**, and the encapsulation yield is tested by measuring the fluorescence intensity of the samples after centrifugation (20 000 g, 10 min). All the samples are prepared with the same amount of QD and with a constant (total ligand/QD) ratio equal to 2000 equivalents. In the presence of an increasing amount of **14**, the fluorescence intensity of the quantum dots micelles increases until reaching a plateau at 10% of amine **14** (Figure 3A). Thus, the addition of a small ratio of the amine analog amphiphile in micelles significantly increases the encapsulation yield of the quantum dots as well as their colloidal stability (see Figure G in the Supporting Information). The minimum value to reach an efficient colloidal stabilization corresponds to a ratio of 10% amine **14**, due to electrostatic repulsion between surface ammonium charges. The comparison between the fluorescence intensity of QD$_{605}$ before and after micellization (QD$_{605}$ micelles) gives rise to the incorporation yield at each purification step.

To evaluate the surface charge of the micelles, we carried out gel electrophoresis migration of quantum dots or hybrid micelles including various ratios of amines on agarose gel. As shown in Figure 3B, the shift of the migration bands of the QD$_{605}$ and γ-Fe$_2$O$_3$/QD$_{605}$ micelles is proportional to the initial ratio of amine/alcohol ligands used. As a control experiment the same experiments are performed with negatively charged **19/17** micelles. In this case, micelles contain-
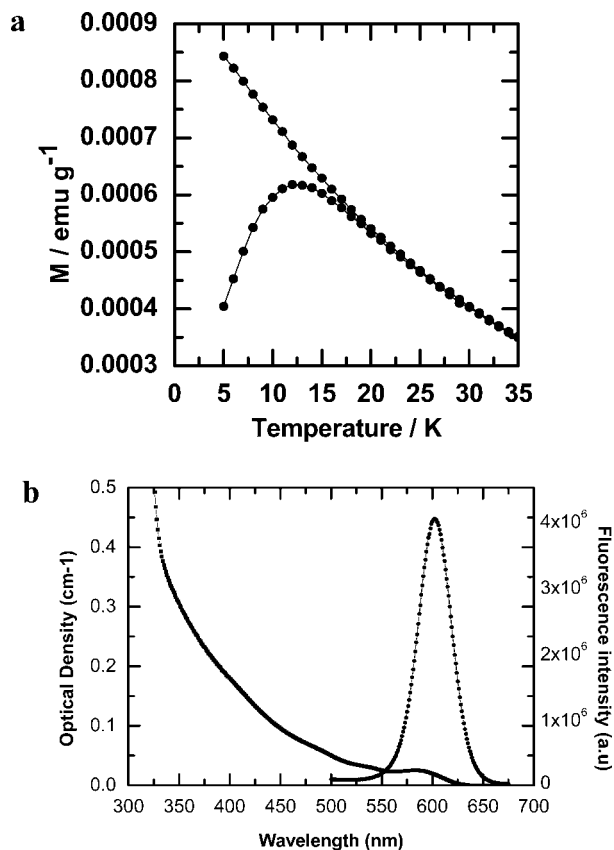

Figure 4. (a) Zero-field-cooled (ZFC) and field-cooled (FC) magnetization curves of a suspension of 1/1 γ-Fe$_2$O$_3$/QD$_{605}$ (**14/17** 10:90) hybrid micelles in water; (b) fluorescence (diamond) and absorption (square) spectrum of the same sample (λ_{exc}= 350 nm).

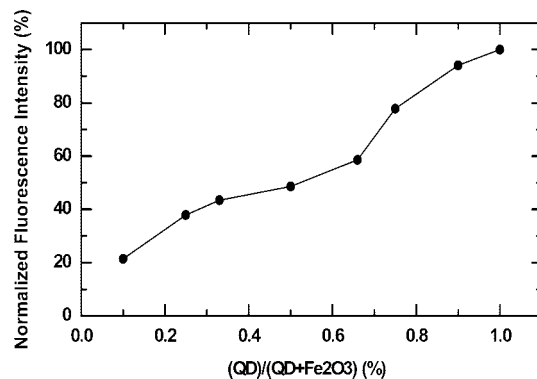**Figure 5.** Evolution of the fluorescence quantum yield with the increase of the QD ratio in γ-Fe$_2$O$_3$/QD$_{605}$ (**14/17** 10:90) micelles.

ing an increasing ratio of negatively charged carboxylate compound **19** exhibit a similar behavior on agarose gel to that of amine **14/17** micelles. Interestingly, the size of the negatively charged micelles is significantly smaller, the hydrodynamical diameter is 20 ± 2 nm and the migration of the negatively charged micelles on electrophoresis gel is larger than for the positively charged micelles (see Figures E and H in the Supporting Information). In the case of the positively charged micelles, the final size of the micelles does not significantly change with the ratio of the amine until 50% (see Figure G in the Supporting Information). Therefore, the observed increasing shift of the band with the amine ratio corresponds to the higher electrophoretic mobility of the positively charged nanoparticles. Up to this concentration,
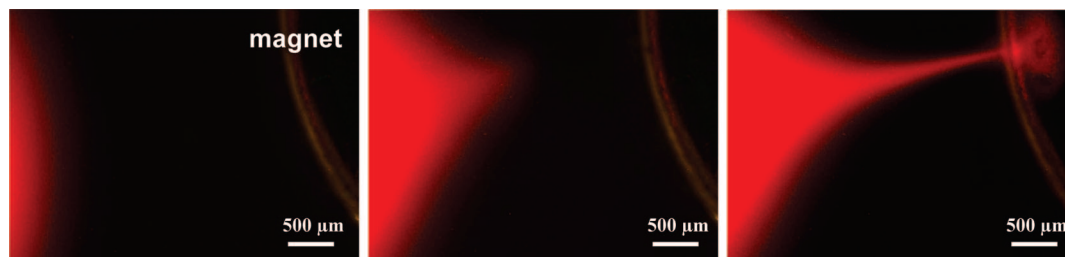
Small Bioactivated Magnetic QD Micelles

Chem. Mater., Vol. 20, No. 21, 2008   6663

Figure 6. Migration of γ-Fe$_2$O$_3$/QD$_{605}$ (**14/17** 10:90) micelles in water (on the left) under permanent magnetic field induced by a cylindrical permanent magnet (on the right side), after 0, 7, and 10 min.
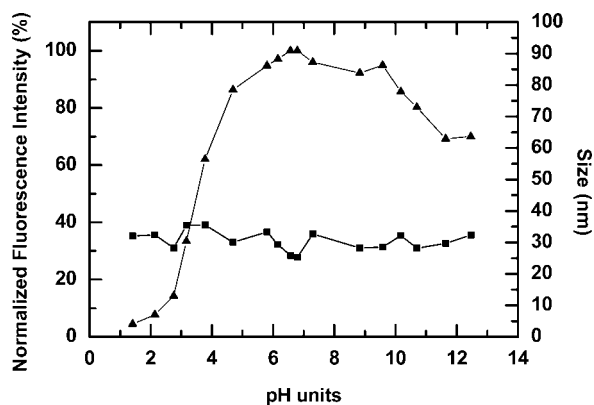

Figure 7. Evolution of the fluorescence intensity (triangle) and the mean diameter (square) during the acido-basic titration of γ-Fe$_2$O$_3$/QD$_{605}$ (**14/17** 10:90) hybrid micelles (100 nM) containing QD$_{605}$ and γ-Fe$_2$O$_3$ in 150 mM NaCl solution.

the migration becomes broad and finally vanishes for the 100% amine ratio. In the latter case, the micelles appear to be destabilized. Thus the present method provides small hybrid micelles with various positive or negative surface charges in one-step process with a control of the micelle charge.

Optical and Magnetic Properties of Hybrid γ-Fe$_2$O$_3$/ QD Micelles (14/17 10:90). Regarding the magnetic properties, the temperature dependence of the magnetization of the γ-Fe$_2$O$_3$/QD$_{605}$ micellar solution has been measured in zero-field-cooled (ZFC) and field-cooled (FC) modes within an applied field of 100 Oe (Figure 4a). The curves are very similar to that obtained for hydrophobic γ-Fe$_2$O$_3$ nanocrystals in cyclohexane (Figure D in the Supporting Information). In ZFC mode, the magnetization exhibits a broad maximum at T_{max} = 13 K characteristic of the freezing of superparamagnetic nanoparticles due to magnetic anisotropy. On cooling, the FC magnetization values are identical to that of ZFC magnetization at higher temperatures than 22 K and then split. This behavior is characteristic of monodisperse and noninteracting nanocrystals. From the saturation value of magnetization at 50 000 Oe and 2 K (M_{sat} = 0.756 emu g^{-1}), it is possible to extract the nanoparticle concentration assuming: (i) the saturation magnetization per chemical unit γ-Fe$_2$O$_3$ is identical to bulk maghemite (M_{sat} = 3.3 Nβ), (ii) the average diameter of the nanoparticles is equal to 4 nm. The nanoparticle concentration deduced from magnetic measurements is 52 μM, whereas that from inductive coupled plasma (ICP) analysis the concentration is found to be 67 μM nanoparticles (i.e., 0.083 M of iron). The difference can

be easily understood by the reduction of the saturation magnetization in nanoparticles due to surface effects.[40]

Concerning the optical properties, the absorption and the emission spectra of the hybrid 1/1 γ-Fe$_2$O$_3$/QD$_{605}$ micelles (**14/17** 10:90) are shown in Figure 4b. A quenching of the QD fluorescence was observed in presence of an increased ratio of γ- Fe$_2$O$_3$ nanocrystals as shown in Figure 5. This quenching is attributed to the recovering of the absorption spectra of the γ-Fe$_2$O$_3$ nanoparticles and the QD$_{605}$ in the near UV domain (around 350 nm). The fluorescent quantum yield decreases with the increasing amount of γ- Fe$_2$O$_3$ for a constant number of QD and for a constant ratio of 2000 equivalents of ligand per 1. The magnetization data have been corrected from diamagnetic contribution of the sample holder (quartz tube) and from the diamagnetism of the solvent (cyclohexane) nanoparticle. The fluorescence quantum yield is about 27 $\pm$ 2% for QD$_{605}$ micelles with only quantum dots and 15 $\pm$ 2% for the γ-Fe$_2$O$_3$/QD$_{605}$ micelles containing a 1/1 ratio of both magnetic and fluorescent particles. In comparison, the QD$_{605}$ quantum yield measured in CHCl$_3$ is 41%. Such a fluorescent quenching was previously observed in the case of magnetic silanized γ-Fe$_2$O$_3$ QDs or FePt-CdS QDs[41,42] Consequently, it is possible to adjust the ratio between magnetic and fluorescent particles in order to find the best condition to keep the acceptable quantum fluorescence yield for imaging application.

To demonstrate the synergy of magnetic and fluorescent nanocrystals, we analyzed the effect of a magnetic field gradient in presence of a permanent magnet (1.25 T) by optical fluorescence microscopy in the case of a 1/1 γ-Fe$_2$O$_3$/ QD$_{605}$ micelles. The magnet induces the migration of the hybrid micelles as shown in Figure 6 within less than 10 min. As a control, no displacement due to Brownian diffusion is observed without the magnet and during the observation time (10 min). After removing the magnetic field, a very slow broadening due the diffusive Brownian movement of the fluorescence zone is observed until reaching a homogeneous distribution. As expected, the migration speed increases while the magnetic gradient becomes stronger as demonstrated by the formation of a cone of fluorescent micelles pointed to the border of the magnet. The application of the magnetic field results in the accumulation of the

(40) Vidal, J.; Rivas, J.; Lopez-Quintela, M. A. *Colloids Surf., A* **2006**, *288*, 44–55.
(41) Gu, H.; Zheng, R.; Zhang, X.; Xu, B. *J. Am. Chem. Soc.* **2004**, *126* (18), 5664–5665.
(42) Selvan, S. T.; Patra, P. K.; Ang, C. Y.; Ying, J. Y. *Angew. Chem., Int. Ed.* **2007**, *46* (14), 2448–2452.
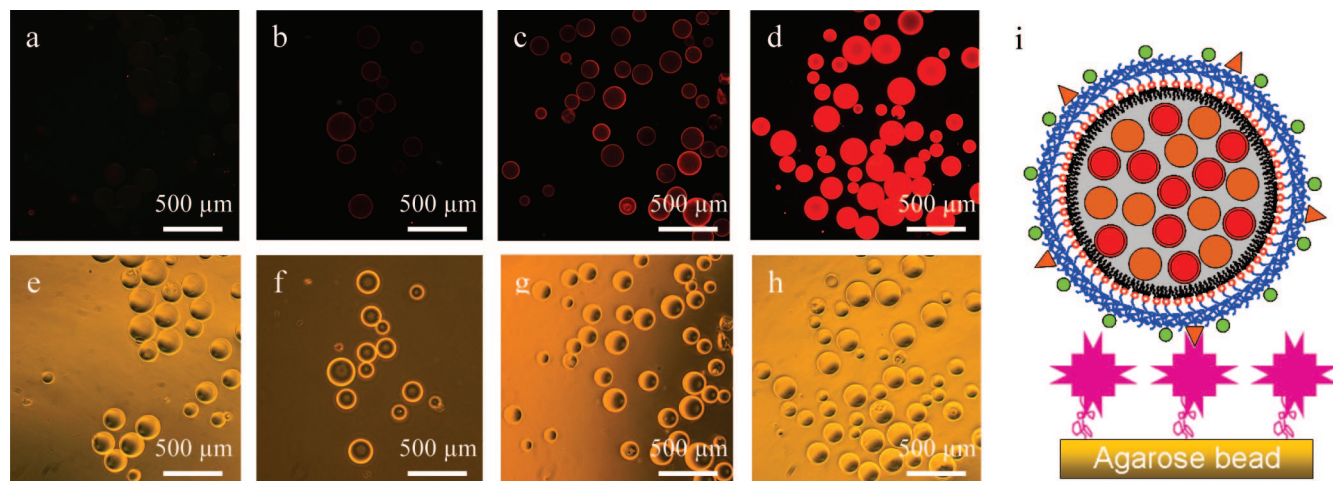
Figure 8. Agarose beads coated with Streptavidin, in presence of micelles **18/14/17** x:10:90−x (images a−e), direct light 5 ms, epifluorescence 300 ms), with an increasing ratio x of **18**: (a, e) 0, (b, f) 0.005, (c, g) 0.05, and (d, h) 0.5%; (i) schematic view of a hybrid biotinylated micelle bound to an immobilized streptavidin (QD$_{605}$ (red sphere), γ-Fe$_2$O$_3$ (brown sphere), **14** (green dots) and **18** (orange triangle) and Streptavidin (purple).

nanoparticles at the magnet surface. This localization can be reversed by removing the magnetic field.

Thus the use of gallate amphiphiles permits to prepare small hybrid fluorescent magnetic micelles of around 25 nm diameter composed of both γ-Fe$_2$O$_3$ and QD and bearing a well-defined number of charged functional amino or carboxylic acid groups that can be further conjugated to biomolecules. In addition, the incorporation of PEG spacer preserves their nonspecific absorption onto any surface and makes possible their use in biological medium.

Stability of γ-Fe$_2$O$_3$ and QD Hybrid Micelles. To validate their potential application in biological medium, we investigated the photostability and the colloidal stability with an increasing ionic strength and various pH. Normalized fluorescence of QD$_{605}$ as well as the mean hydrodynamical size of the micelles is measured over a period of a month to estimate quantitatively the stability of the micelles in saline solution with various ionic strengths (see Figure I in the Supporting Information). No tendency to aggregation is observed with an increasing ionic strength up to 1 M (data not shown) but the fluorescence appears to be sensitive over some days. The photostability in function of the pH (see Figures J and K in the Supporting Information) is then investigated over a 1 month time period. The hybrid micelles are found to be stable in fluorescence and in size at neutral and basic pH. On the contrary, a strong quenching of the fluorescence is observed in acid medium, below pH 4 (see Figure 7), while the size is maintained constant. Thus the observed quenching is not due to a colloidal destabilization. Photostability over 1 month is observed in classical buffer such as HEPES (pH 7.5) and boric buffer (pH 8.5) with 150 mM NaCl and 20 mM buffer (see Figure K in the Supporting Information) closed from the physiological conditions. Therefore, the micellization process prevents colloidal destabilization as well as any significant fluorescence extinction in presence of a basic buffer (pH between 7 and 8.5).

Bioactivation. To demonstrate their ability to target a biomolecule, hybrid fluorescent and magnetic γ-Fe$_2$O$_3$/QD$_{605}$ micelles are slightly modified to include the biotinylated ligand **18**. Hybrid fluorescent and magnetic γ-Fe$_2$O$_3$/QD$_{605}$ micelles are prepared from a ligand mixture containing various molar percentages of **18** and a 10:90 mixture of **14** and **17**. The obtained micelles exhibit the same properties as those of amine **14/17** micelles in terms of hydrodynamic size, fluorescence, and colloidal stability. After incubation of the Biotin tagged γ-Fe$_2$O$_3$/QD$_{605}$ hybrid micelles with immobilized Streptavidin agarose beads, and extensive washing to remove the excess γ-Fe$_2$O$_3$/QD$_{605}$ micelles, the fluorescence of the agarose beads is observed only in the presence of biotin at the surface of the hybrid micelles by epifluorescence microscopy (Figure 8). The binding of biotinylated micelles is detected with a ratio ranging from 0.5 to 0.005% of **18**. In addition, very little nonspecific adsorption is observed using pure amine/alcohol (**14/17** 10: 90) micelles. This simple experiment demonstrates the ability of the hybrid γ-Fe$_2$O$_3$/QD$_{605}$ micelles to be used to target proteins. Interestingly, it might be possible to reduce the number of active biotin group per QD. The biotin/streptavidin interaction is enough strong to reduce the biotin ratio to 0.005 mol % so that is closed to a mean ratio to one biotin ligand per micelle. Such hybrid micelles could be used to conjugate any biotinylated biomolecule and get the ideal 1:1 stoichiometry suited for biolabeling and tracking of a single protein.

Conclusion

In conclusion, pegylated hybrid magnetic and fluorescence micelles with a 25 nm diameter are obtained starting from simple mixtures of amine, carboxylic or biotin and alcohol gallate amphiphiles. The structural properties of the self-assembled amphiphiles are correlated to their ability to encapsulate the nanocrystals. The main presence of the hexagonal direct phase is required to observe the formation of isolated hybrid QD magnetic micelles. These hybrid micelles can be prepared with a controlled ratio of active groups (amino, carboxylic acid, or biotin) at their surface, and therefore it is possible to control their charge and the number of reactive sites per micelle. Their colloidal stability under various conditions of pH and saline buffers as well as their optical and magnetic properties were deeply analyzed and demonstrate their ability to be used to track and trap biomolecules. The efficiency of the biotin/Streptavidin molecular recognition is clearly demonstrated on Streptavidin

immobilized agarose microbeads and permits us to consider the use of such hybrid magnetic fluorescent micelles to target and manipulate proteins in biological medium and investigate the possibility to modulate the signalization pathways involved in many biological processes of self-organization. Our method to target biomolecules with magnetic and fluorescent gallate amphiphile micelles under physiological conditions will be next applied to proteins of interest in living cells.

Supporting Information Available: (1) Small-angle X-ray scattering (SAXS) spectra of **15**, **16**, and **17** $G_{11}EO_nOH$ ($n = 8$, 23, 34) into a water gradient (Figures A1−3); (2) summary table of the fusion temperatures and molar formation enthalpies of the pure **17** and $G_{12}EO_{34}OH$ compounds with or without water extracted from differential scanning calorimetry (Table A); (3) experimental procedures of nanocrystals and gallate amphiphiles synthesis; (4) size histogramms of the nanocrystals obtained by TEM experiments (Figures B and C); (5) magnetization curve of magnetic hydrophobic γ-Fe_2O_3 nanocrystals (Figure D); (6) size distribution of the hybrid micelles obtained by DLS (Figure E); (7) typical images of γ-Fe_2O_3 micelles and QD micelles obtained by TEM (Figure F); (8) electrophoresis gels of various negatively charged QD micelles composed of a mixture **19/17** (Figure H); (9) colloidal stability of hybrid micelles upon ratio of amine **14**, ionic strength, and pH (Figures G, I, J, K) (PDF). This material is available free of charge via the Internet at http://pubs.acs.org.

CM801423R